Clim Dyn
DOI 10.1007/s00382-015-2601-6

Spatiotemporal characteristics and synchronization of extreme rainfall in South America with focus on the Andes Mountain range

Niklas Boers[1,2] · Bodo Bookhagen[3] · Norbert Marwan[1] · Jürgen Kurths[1,2,4,5]

Received: 30 January 2015 / Accepted: 6 April 2015

Abstract The South American Andes are frequently exposed to intense rainfall events with varying moisture sources and precipitation-forming processes. In this study, we assess the spatiotemporal characteristics and geographical origins of rainfall over the South American continent. Using high-spatiotemporal resolution satellite data (TRMM 3B42 V7), we define four different types of rainfall events based on their (1) high magnitude, (2) long temporal extent, (3) large spatial extent, and (4) high magnitude, long temporal and large spatial extent combined. In a first step, we analyze the spatiotemporal characteristics of these events over the entire South American continent and integrate their impact for the main Andean hydrologic catchments. Our results indicate that events of type 1 make the overall highest contributions to total seasonal rainfall (up to 50 %). However, each consecutive episode of the infrequent events of type 4 still accounts for up to 20 % of total seasonal rainfall in the subtropical Argentinean plains. In a second step, we employ complex network theory to unravel possibly non-linear and long-ranged climatic linkages for these four event types on the high-elevation Altiplano-Puna Plateau as well as in the main river catchments along the foothills of the Andes. Our results suggest that one to two particularly large squall lines per season, originating from northern Brazil, indirectly trigger large, long-lasting thunderstorms on the Altiplano Plateau. In general, we observe that extreme rainfall in the catchments north of approximately 20°S typically originates from the Amazon Basin, while extreme rainfall at the eastern Andean foothills south of 20°S and the Puna Plateau originates from southeastern South America.

Keywords Extreme rainfall · Synchronization · Complex networks · South American monsoon system

✉ Niklas Boers
boers@pik-potsdam.de

[1] Potsdam Institute for Climate Impact Research, Telegraphenberg A 31, 14473 Potsdam, Brandenburg, Germany

[2] Department of Physics, Humboldt University Berlin, Berlin, Germany

[3] Institute of Earth- and Environmental Sciences, University of Potsdam, Brandenburg, Germany

[4] Department of Control Theory, Nizhny Novgorod State University, Nizhny Novgorod, Russia

[5] Institute for Complex Systems and Mathematical Biology, University of Aberdeen, Aberdeen, UK

1 Introduction

The South American Andes are exposed to intense rainfall events that often lead to landslides and downstream flooding, with severe socio-economic impacts (Moreiras 2005; Harden 2006; Barros et al. 2006; PNUD 2011). These events frequently occur as large and long-lasting thunderstorms. Characteristic examples are the so-called Amazonian squall lines (Cohen et al. 1995) in the tropics, as well as mesoscale convective systems (Maddox 1980; Griffiths et al. 2009; Romatschke and Houze 2013; Boers et al. 2013), which attain largest spatial scales in subtropical South America (Velasco and Fritsch 1987; Durkee and Mote 2009a, c; Durkee et al. 2009; Romatschke and Houze 2010; Rasmussen and Houze 2011).

During the monsoon season from December to February, the southward displacement of the Intertropical Convergence Zone as well as differential heating between ocean and land leads to enhanced easterly moisture inflow from

Published online: 18 April 2015

the tropical Atlantic ocean to the South American continent (Zhou and Lau 1998; Vera et al. 2006). After crossing the Amazon basin, these low-level winds are blocked by the Andes, where their interplay with the orography is responsible for intense, orographic rainfall and associated floodings at the eastern slopes of the tropical (i.e., northern and northern Central) Andes (Bookhagen and Strecker 2008; Houze 2010). The mountain range forces the winds southward, leading to the establishment of the South American Low-Level Jet (Marengo et al. 2004; Poveda et al. 2014). This wind system leads to further orographic rainfall at the eastern slopes of the Central Andes (Bookhagen and Strecker 2008; Houze 2010), but also provides the moisture necessary for the formation of mesoscale convective systems in subtropical South America (Salio et al. 2007). Large rainfall clusters frequently propagate from the subtropical plains towards the Andes, causing severe flooding and landsliding events at the eastern slopes of the subtropical Andes (Boers et al. 2014a).

The local characteristics of extreme rainfall in terms of their frequency distribution has been thoroughly studied in the literature (e.g. Renard et al. 2013; Papalexiou and Koutsoyiannis 2013; Serinaldi and Kilsby 2014). Statistical analysis of the temporal durations and spatial extensions of extreme rainfall events in South America as well as their hydrological importance have, for example, been been studied in Khan et al. (2007), Romatschke and Houze (2010), Rasmussen and Houze (2011). The specific contribution of mesoscale convective complexes in subtropical South America to the total rainfall budget has been analyzed in Durkee et al. (2009). However, the dynamical synchronization properties of extreme rainfall events, whilst taking into account their spatiotemporal characteristics, need to be known for a robust assessment of their geographical origins. This becomes particularly relevant when identifying the sources of extreme rainfall in given river catchments. Here, we focus on four different types of rainfall events: (1) events which are solely determined by their high magnitude; (2) events which are characterized by their long duration *and* high magnitude; (3) spatially extensive events; and (4) high magnitude, long-lasting and spatially extensive events.

In a first step, using high spatiotemporal resolution satellite rainfall data, we analyze the frequencies, intensities, and spatial extensions of the four proposed event types. In addition, we quantify their respective contribution to the overall water budget of the main drainage basins along the Andean mountain range, including several sub-basins of the Amazon and the La Plata rivers.

We are particularly interested in the spatial scales of rainfall clusters. The size of these clusters will be determined by the number of grid cells belonging to a connected component of simultaneous events and we will analyze the

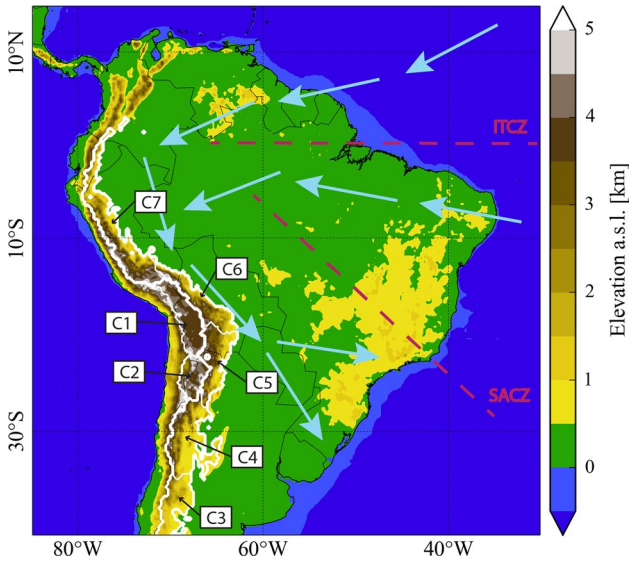

Fig. 1 Topography of South America derived from Shuttle Radar Topography Mission (SRTM) data (Farr et al. 2007), as well as the climatological positions of the Intertropical and South Atlantic Convergence Zones (ITCZ and SACZ) and typical low-level wind directions for the DJF season. The seven catchments C1 to C7 referred to in the text are delineated by *white contour lines*. The labels refer to the Altiplano plateau (*C1*), the Puna de Atacama plateau (referred to as the Puna) (*C2*), and river catchments at the eastern slopes of the southern (*C3*), southern Central (*C4*), Central (*C5*), northern Central (*C6*), and northern Andes (*C7*)

frequency distribution of these cluster sizes. The employed gauge-calibrated satellite product TRMM 3B42 V7 is considered to provide high-quality estimates of rainfall variability in South America (Carvalho et al. 2012; Zulkafli et al. 2014; Boers et al. 2013), but also in other regions of the earth (Xue et al. 2013; Chen et al. 2013). Its high spatiotemporal resolution is essential for the study of extreme events and the spatial patterns of their synchronization using complex networks.

In a second step, we investigate the geographic source areas of the four types of rainfall events for the mountainous Andean drainage basins, including the high-elevation Altiplano-Puna Plateau. The spatiotemporal characteristics of rainfall events on the Altiplano-Puna Plateau are crucial for understanding and sustaining water resources in this region. While this area forms an almost continuous topographic plateau with a mean elevation of 4041 ± 524 m and constitutes the second-largest plateau on earth (after the Tibetan Plateau), the geomorphic and climatic characteristics of its northern and southern parts are distinct (Messerli et al. 1997; Vuille 1999; Garreaud and Aceituno 2001; Garreaud et al. 2003; Bookhagen and Strecker 2012). We therefore divide this arid 1800 km long and 350 to 400 km wide region into the northern Altiplano (C1) and the southern Puna de Atacama (C2) Plateaus (Fig. 1). In addition to

the high-elevation Altiplano-Puna Plateau, the origins of extreme rainfall are of particular hydrological importance in the mountainous drainage basins along the Andes. We will divide them into five sub-catchments roughly corresponding to the southern Andes (C3), the southern Central Andes (C4), the Central Andes (C5), the northern Central Andes (C6), and the northern Andes (C7) (Fig. 1). We will occasionally refer to the northern and northern Central Andes (C6 and C7) as tropical, and to the remaining southern parts as subtropical.

In order to determine the geographical origins of extreme rainfall in these river catchments, we employ and refine a recently introduced statistical method based on a non-linear synchronization measure and complex network theory. While so-called *climate networks* have been applied to a wide range of meteorological and climatological problems (Tsonis et al. 2006; Yamasaki et al. 2008; Donges et al. 2009; Steinhaeuser et al. 2012; Berezin et al. 2012; Radebach et al. 2013), the specific methodology employed here has proven to be particularly useful for the climatological analysis of extreme rainfall (Malik et al. 2012; Boers et al. 2013, 2014a, b, c, 2015; Rheinwalt et al. 2014; Stolbova et al. 2014), because it is specifically designed to uncover temporally resolved interdependencies of extreme events in the presence of non-linearities and strongly non-Gaussian data distributions. Here, we further generalize this approach in order to take into account different temporal and spatial scales of rainfall events. For this purpose, we first carry out several steps of temporal and spatial pre-processing. Furthermore, we refine the directed network approach first introduced in Boers et al. (2014a) to identify geographical source regions. Using this framework, we then resolve the source regions of rainfall in the mountainous Andean catchments (C1–C7) with respect to the four types of rainfall events described above. We note that our approach is conceptually different from techniques like Lagrangian backtracking, since it does not analyze the actual moisture transport process. Instead, our method identifies spatial linkages to locations where extreme rainfall occurs synchronously with extreme rainfall in a region under consideration, while taking into account the temporal order of rainfall events and assuring that the association of events is unique and statistically significant.

2 Data

We employ the gauge-calibrated remote-sensing derived rainfall dataset TRMM 3B42 V7 of the Tropical Rainfall Measurement Mission (Huffman et al. 2007) for the time period from 1998 to 2012 for the spatial domain 15°N to 40° S and 85°W to 30°W. The spatial resolution of this dataset is $0.25° \times 0.25°$, and the temporal resolution is 3 hours. For each 3-hourly time step, the data is provided as average rainfall rate in units of [mm/h]. River catchments have been delineated from resampled topographic data [Shuttle Radar Topography Mission, (Farr et al. 2007)] at a spatial resolution of 15 arcseconds (≈500 m).

3 Methods

3.1 Definition of extreme events

We will focus on the monsoon season in South America from December to February (DJF) and analyze the following three different spatial and temporal characteristics of 3 -hourly rainfall events: Their *intensity*, *duration*, and *spatial extent*.

Existing climate networks approaches to analyze extreme rainfall synchronization are either based on a fixed threshold or on a percentile score to determine extreme events in each time series, without taking into account the temporal and spatial scales of these events (e.g. Malik et al. 2012; Boers et al. 2013, 2014a). Here, we explicitly disentangle the impacts and origins of extreme rainfall in the main Andean drainage basins with respect to their intensity, duration, and spatial extent. For this purpose, we estimate the temporal duration of each event, dynamically record the sizes of the associated rainfall storms, and finally combine the thereby obtained temporal and spatial information of rainfall events. Depending on these characteristics, we apply several steps of preprocessing:

1. Let the rainfall time series at location i be denoted by $\tilde{t}_i$, where $1 \leq i \leq N = 48{,}400$. We can apply a running-mean filter in order to account for the temporal duration of rainfall events:

$$t_i^\sigma := \frac{\sum_{s=-w}^{w} \tilde{t}_i^{\sigma+s}}{2w+1},$$

where σ is the time index and $2w+1$ is the width of the running-mean filter. For ease of notation, we omit making the dependency of t_i^σ on w explicit. The application of this running-mean filter will in the following be referred to as *smoothing*.
2. For each filtered time series t_i, we define local event thresholds T_i^p by computing the pth percentile of all t_i^σ with $t_i^\sigma > 0.2$ mm. The latter condition assures that only significant rainfall amounts ("wet times") are taken into account when computing the percentile thresholds. *Local events* are then defined as time steps σ for which t_i^σ is above this threshold:

$$\tilde{e}_i := \{\sigma | t_i^\sigma > T_i^p\}$$

Again for the sake of clarity, we omit to make explicit that $\tilde{e}_i$ depends on w as well as on p.

3. We are also interested in the spatial extent of events, given by the size of connected components $\{\mathcal{C}_m^\sigma\}_{1\leq m\leq N_\sigma}$ with simultaneous events $\tilde{e}_i$ at a given time σ. Here, grid points are considered to be connected if they are (also diagonally) adjacent in space, and N_σ denotes the total number of connected components at time step σ. To each grid point i, we then assign the size of the component it belongs to:

$$SC_i^\sigma = \sum_{\{\mathcal{C}_m^\sigma\}} \delta_{\mathcal{C}_m^\sigma}(i)|\mathcal{C}_m^\sigma|\,,$$

where $|\mathcal{C}_m^\sigma|$ denotes the cardinality of $\mathcal{C}_m^\sigma$ (i.e., the number of elements in that set) and $\delta_{\mathcal{C}_m^\sigma}(i) = 1$ if $i \in \mathcal{C}_m^\sigma$ and $\delta_{\mathcal{C}_m^\sigma}(i) = 0$ otherwise. We then define a component size threshold S_i^q at each grid cell i as the qth percentile of all SC_i^σ for which $SC_i^\sigma > 0$ (i.e., the qth percentile of the set $\{SC_i^\sigma\,|\sigma \text{ such that } SC_i^\sigma > 0\}$). We then define *spatially extensive events* as local events which belong to a connected component that is larger than the corresponding S_i^q:

$$e_i := \{\tilde{e}_i | SC_i^{\tilde{e}_i} > S_i^q\}\,,$$

which depends on the width of the temporal filter w, the intensity threshold T_i^p, and the threshold for the cluster size S_i^q.

We define the following four types of events that we will analyze in the following sections:

1. Local and short extreme events (LSE), which are intense rainfall events (high magnitude), regardless of their duration and spatial extent: $w = 0$, $p = 90$, and $q = 0$
2. Local and long-lasting extreme events (LLE), which are long-lasting intense rainfall events, but without condition on their spatial extent: $w = 5$, $p = 90$, and $q = 0$
3. Spatially extensive events (SEE), which are not necessarily very intense or long-lasting: $w = 0$, $p = 50$, and $q = 90$
4. Spatially extensive and long-lasting extreme events (SLE): $w = 5$, $p = 90$, and $q = 90$

We note that these four definitions are deliberately not disjoint, i.e., given events may be part of two or more of these classes. The reason for this is that for a given event type, we are interested in the characteristics of all events of that type, in contrast to the characteristics of events which only fulfill the conditions of one event type, but none of the conditions of the remaining three event types.

We further emphasize that by *events* we always refer to 3 -hourly time steps, and not to the possibly longer or shorter period of consecutive rainfall above the prescribed threshold. In particular, an event should not be confused with an individual convective storm. Furthermore, the temporal filter introduced above does by definition not quantify the actual duration of a given rainfall storm, but rather assures that the resulting (3-hourly) events belong to persisting high-rainfall periods, since they still exhibit high values after being smoothed by a 15-h running mean ($w = 5$ for LLE and SLE). The reason for defining events like this is that in order to apply the synchronization measure which will be introduced in the following, it is crucial to have all events at the same time scale.

3.2 Event synchronization

In order to quantify the synchronicity of events at different locations, we employ *event synchronization* (ES), a nonlinear measure which we define based on Quiroga et al. (2002), Malik et al. (2012), Boers et al. (2013):

Suppose we have two event series $\{e_i^\mu\}_{1\leq\mu\leq l_i}$ and $\{e_j^\nu\}_{1\leq\nu\leq l_j}$ with l_i (l_j) events at grid points i (j). As explained in the last section, e_i^μ denotes the time index of the μ-th event observed at grid point i. In order to decide if two events e_i^μ and e_j^ν can be uniquely assigned to each other, we compute for the waiting time $d_{ij}^{\mu,\nu} := e_j^\nu - e_i^\mu$ between two events the *dynamical delay*

$$\tau_{ij}^{\mu\nu} := \min \frac{\{d_{ii}^{\mu-1,\mu}, d_{ii}^{\mu,\mu+1}, d_{jj}^{\nu-1,\nu}, d_{jj}^{\nu,\nu+1}\}}{2}.$$

To exclude unreasonably long delays between events at different locations, we introduce a maximum delay of $\tau_{max} = 8$ time steps (i.e., one day). If $0 < d_{ij}^{\mu,\nu} \leq \tau_{ij}^{\mu\nu}$ and $0 < d_{ij}^{\mu,\nu} < \tau_{max}$, we count them as synchronous events in a way that the event at i happened before the event at j:

$$S_{ij}^{\mu\nu} = \begin{cases} 1 & \text{if} \quad 0 < d_{ij}^{\mu,\nu} \leq \tau_{ij}^{\mu\nu} \quad \text{and} \quad 0 < d_{ij}^{\mu,\nu} \leq \tau_{max}, \\ 0 & \text{else.} \end{cases}$$

ES between e_i and e_j for events at i occurring before events at j is given as the sum of all $S_{ij}^{\mu\nu}$ (for fixed i and j):

$$ES_{ij} := \sum_{\mu\nu} S_{ij}^{\mu\nu},$$

while the reverse time direction is given by

$$ES_{ji} := \sum_{\mu\nu} S_{ji}^{\mu\nu}.$$

Each value ES_{ij} therefore yields the number of events at grid point j which occurred synchronously (i.e., could be uniquely assigned to each other) with succeeding events at grid point i. This procedure is

performed for all combinations of grid points i and j, with $1 \leq i, j \leq N = 48{,}400$. Note that, by construction, events that occur at the very same time step at different locations are discarded, since they do not allow to determine the temporal ordering of events.

3.3 Construction of complex networks

Most studies employing ES in the context of extreme rainfall use a simple percentile thresholding procedure to determine extreme events, which leads to the same number of events at each grid cell (e.g. Malik et al. 2012; Boers et al. 2013, 2014a). In contrast, the fact that here we define extreme events based on their intensity, temporal, and spatial scales together leads by construction to typically different numbers of events at different grid cells. Since this number of events affects the measured values of ES, we propose the following network construction procedure based on locally adapted statistical null models: For each pair of grid cells (i, j), we first estimate the statistical significance of the values ES_{ji} and ES_{ij} by constructing a null model under the assumption that the l_i events at i and l_j events at j occur independently according to a uniformly random distribution of periods of consecutive events: We independently construct 1000 surrogate pairs of event time series, on average preserving the original distribution of periods of consecutive events and compute ES for all these pairs. In this way, we obtain a relative frequency distribution of values of ES consistent with the assumptions of the null model and infer the score ET of the 95 % significance level from this distribution. A directed network link from grid cell i to grid cell j will be placed if the corresponding value ES_{ij} is above this threshold:

$$A_{ij} = \Theta(ES_{ij} - ET(l_i, l_j)) - \delta_{ij},$$

where Θ denotes the Heaviside function and Kronecker's delta δ is used to exclude self loops.

3.4 Application of complex networks

We will use this combination of ES and complex networks to determine the geographic origins of extreme rainfall in a given region of interest R. This methodological framework is well-suited for this task, since it is designed to reveal possibly non-linear climatic linkages on the basis of event time series. We note that the identification of such geographical source regions is limited by the fact that the thresholding with respect to intensity, duration, and size applies on the entire spatial domain: Any event e_i^{μ} will by construction only be identified as statistically synchronous to a given event e_j^{ν} if it fulfills the same set of defining conditions (types 1–4 above). Possible geographic origins of events of a given type in a given region R will thus be missed if the events in the source region are not of the same type. We define *regional connectivity* of R by counting for each grid point i the number of links pointing into R:

$$RC_i(R) = \sum_{j \in R} A_{ij}$$

This measure yields a value for each grid point i. In order to be able to visualize RC for different regions on the same spatial map, we will in the following use a binary version of this measure: A grid point i will be considered to have strong linkages to a region R if the number of network links pointing from i to R is more than ten times larger than what should be expected from a uniformly random placement of all available links. Note that, compared to Boers et al. (2014a), we hereby expand the presentation of RC by an estimation of statistical significance.

By indicating where rainfall events typically occur *before* they synchronously occur in a region under consideration, RC estimates the geographic *origins* of rainfall events in that region. These directed climatic linkages are helpful for identifying and understanding spatial synchronization patterns of extreme rainfall events, but also provide essential information for assessing the statistical predicability of these events at any region R (e.g. Boers et al. 2014a). In Sect. 4.2, we will investigate these climatic linkages separately for the four different event types proposed above.

4 Results

4.1 Frequency, intensity, and spatial extent of rainfall events

4.1.1 Rainfall intensity

The monsoon season in South America is characterized by high mean rainfall values in the vicinity of the Intertropical Convergence Zone (ITCZ), in the Amazon Basin and along the South Atlantic Convergence Zone (SACZ), as well as along the eastern slopes of the Peruvian and Bolivian Andes (Fig. 2a). The 50th percentile scores of wet times (hourly rainfall larger than 0.2 mm/h) shows highest values at the northeastern South American coast, the eastern slopes of the Bolivian Andes as well as in northern Argentina (Fig. 2b). 90th percentile scores of 3-hourly wet times exhibit highest values at the eastern slopes of the Bolivian Andes and in northeastern Argentina as well (Fig. 2c). While the spatial distribution of 90th percentile scores for 3-hourly wet times of the 15-h smoothed time series (Fig. 2d) resembles that obtained for the non-smoothed case, the assumed values are considerably lower due to the temporal smoothing.

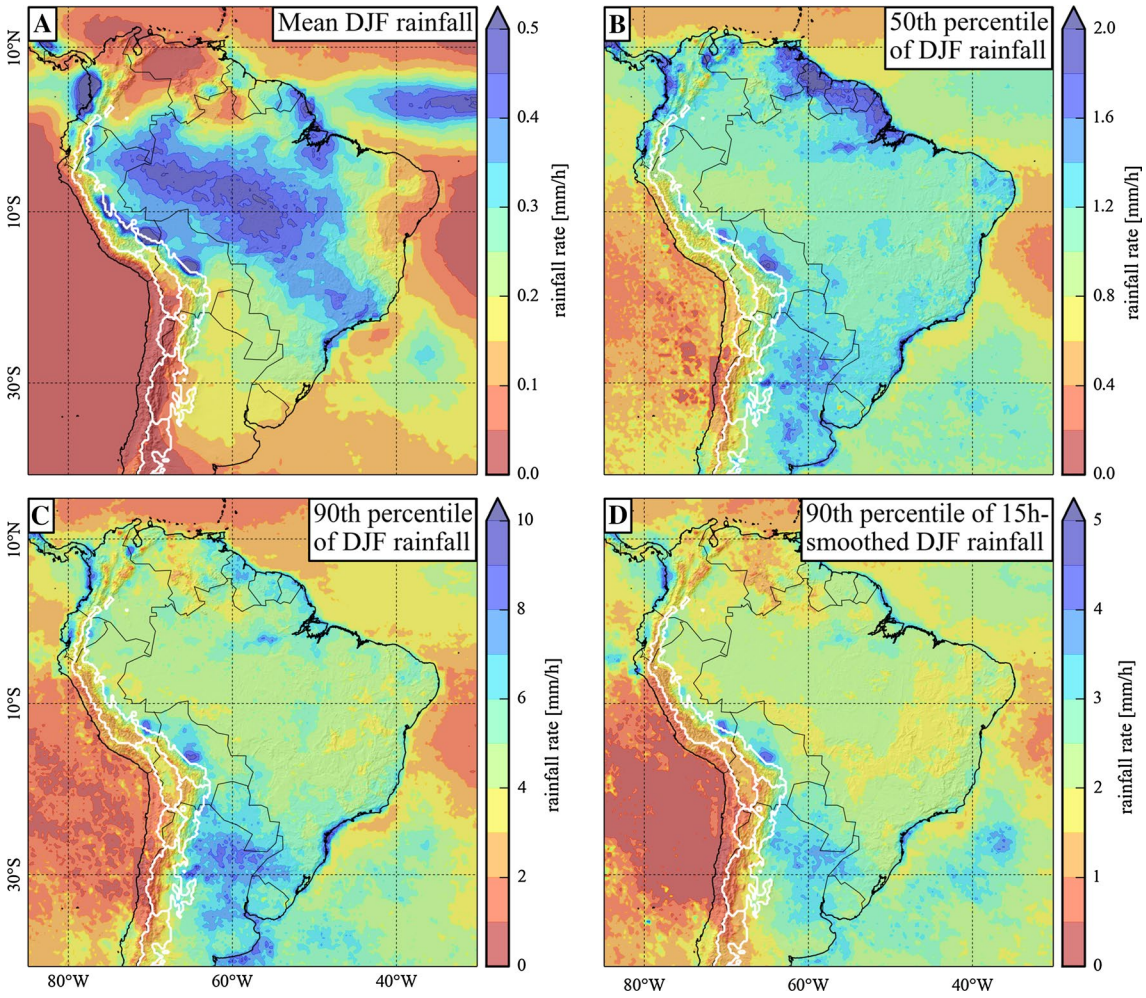

Fig. 2 **a** Mean hourly rainfall for DJF from 1998 to 2012. **b** 50th percentile of rainfall distribution confined to wet times (i.e., 3-hourly time steps with average hourly rainfall larger than 0.2 mm/h). **c** 90th percentile of rainfall distribution confined to wet times. **d** 90th percentile of 15-h smoothed (using a 5-point moving average) rainfall distribution confined to wet times

4.1.2 Frequencies of the four event types

In the previous section, we have defined four types of extreme events that we will analyze in more detail: LSE, LLE, SEE, and SLE. Each event type occurs with different frequencies, although the relative spatial distribution of these frequencies remains similar (Fig. 3). We emphasize that by *frequency*, we refer to the number of 3-hourly time steps which have an event, implying that, e.g., 4 consecutive time steps fulfilling the respective event condition are counted as 4 events.

1. For LSE, we obtain typical values between 12 and 18 events per DJF season in the Amazon Basin and at the eastern Andean slopes north of 20°S, but only around 4 to 6 events in the subtropical plains of southern Bolivia, Paraguay, northern Argentina, and the adjacent Andean slopes (Fig. 3a).
2. For LLE, these numbers are 25–30 and 7–12 respectively (Fig. 3b).
3. For SEE, there are between 7 and 10 events in the Amazon Basin at the slopes of the northern Central Andes and between 1 and 4 events in the subtropical plains (Fig. 3c).
4. For the most extreme SLE, we find 1–4 events in the Amazon Basin and the adjacent foothills of the Andes, but less than one such event per season in the subtropics of northern Argentina and Uruguay (Fig. 3d).

Most notably, for all four event types, we observe a pronounced latitudinal gradient of event frequencies between the tropics and the subtropics: the northern, tropical regions have high event frequencies, while the subtropics exhibit considerably lower frequencies. This gradient can be assumed to be inherited from the mean rainfall profile (Fig. 2a), which exhibits the same characteristic. Similar results

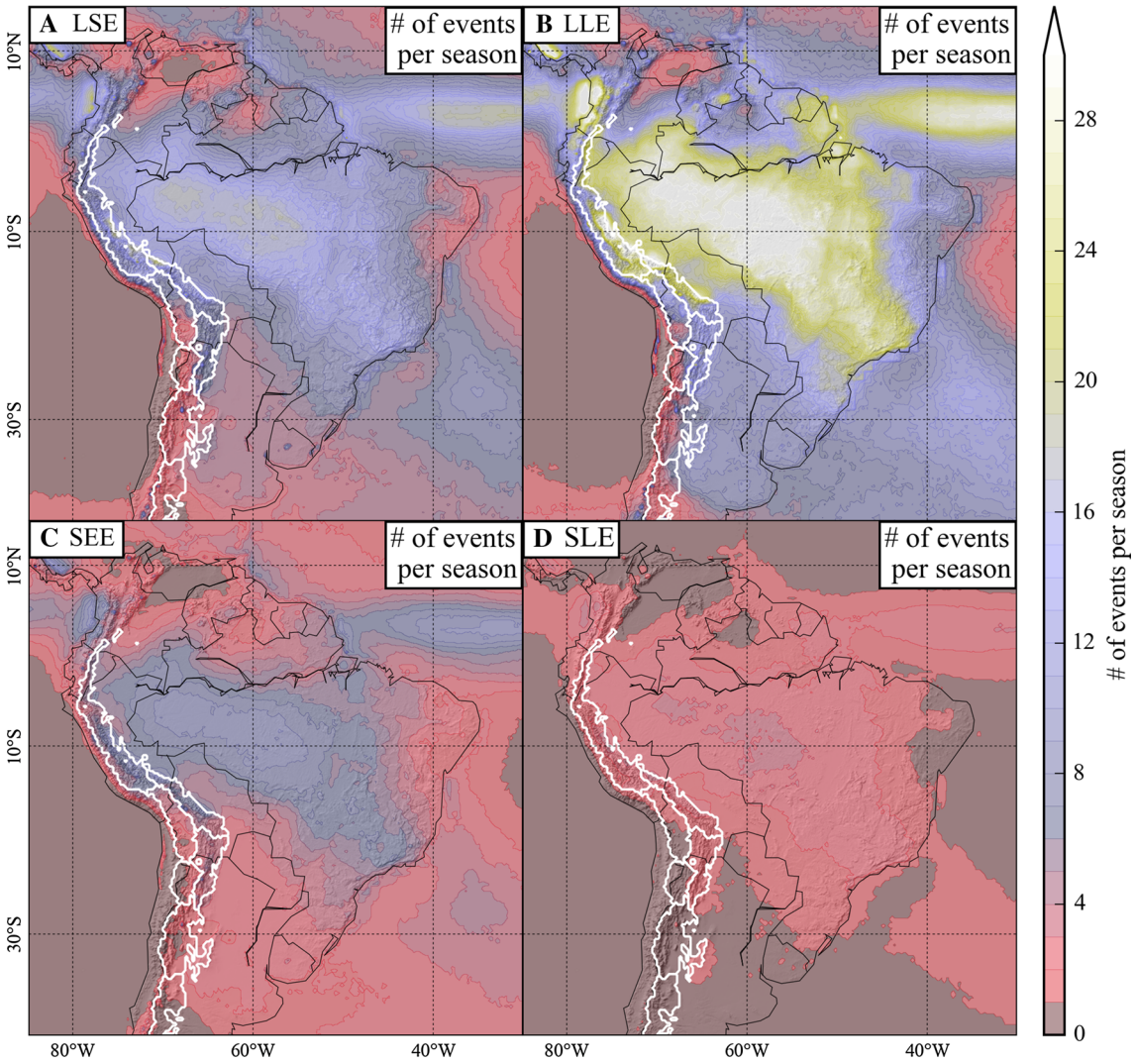

Fig. 3 Number of events per DJF season for local and short extreme events (**a** LSE), local and long-lasting extreme events (**b** LLE), spatially extensive events (**c** SEE), and spatially extensive long-lasting extreme events (**d** SLE)

on the spatial distribution of mean rainfall sums have for example been reported in Durkee et al. (2009), Romatschke and Houze (2010, 2013).

4.1.3 Contributions to total seasonal rainfall

The fraction of total DJF rainfall sums (not confined to wet times) accounted for by the four event types varies considerably:

1. LSE events account for more than 40 % of total seasonal rainfall in large parts of tropical South America, and even more than 50 % in some areas in the subtropics (Fig. 4a).
2. The spatial distribution of total rainfall fractions for LLE is similar to the one obtained for LSE, but local values are about 10 % lower (Fig. 4b).
3. In contrast, SEE account for much lower fractions of total rainfall, with values ranging between 5 and 10 % in most of Brazil, and between 10 and 20 % in the subtropical plains (Fig. 4c).
4. The lowest contributions were found for SLE, with fractions reaching 10 % only in some parts of northern Argentina and Paraguay (Fig. 4d).

As emphasized above, events of all four types are by construction 3-hourly time steps. Consecutive time steps with events will in the following be referred to as *bursts*. We emphasize that typical time scales of duration of the four events types (i.e., the number of events per bursts) vary by definition: bursts of LSE and SEE usually last 3–6 hours (roughly 1–2 events), while for LLE we find typical duration periods of 9–15 h (3–5 events), and SLE last 6–12

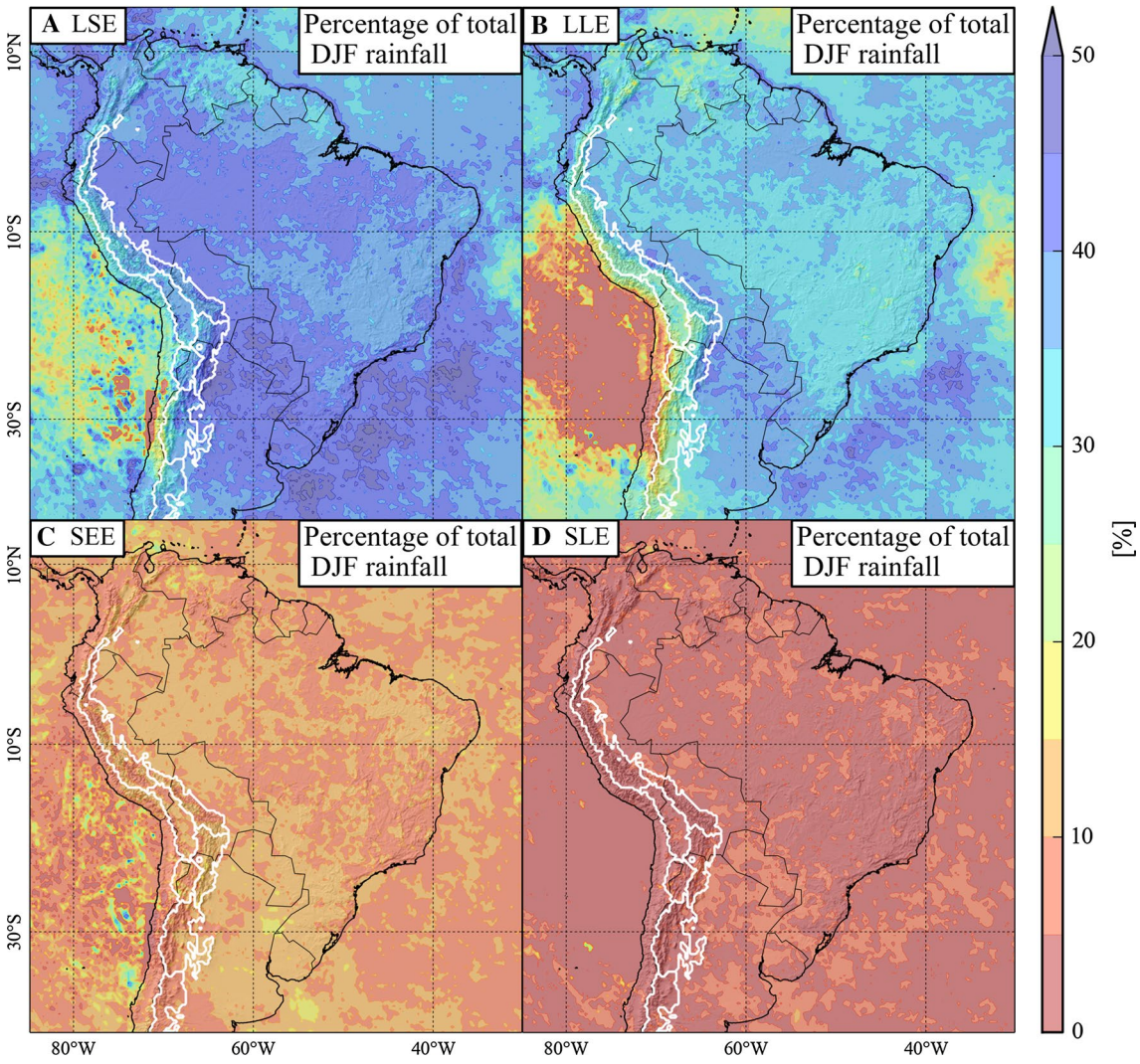

Fig. 4 Percentage of total DJF rainfall contributed by local and short extreme events (**a** LSE), local and long-lasting extreme events (**b** LLE), spatially extensive events (**c** SEE), and spatially extensive long-lasting extreme events (**d** SLE)

h (2–4 events) (cf. Fig. 5). In order to adjust for the varying event frequencies and burst durations when considering fractions of accounted DJF rainfall, we compute the average fraction of total DJF rainfall contributed by a single burst (Fig. 6). To avoid confusion, we remark that Fig. 4 shows the rainfall fractions contributed by all events of the respective type, while Fig. 6 shows the respective contributions by each *single* burst.

1. We find that each LSE burst accounts on average for 3–4 % of total DJF rainfall in the Amazon Basin and the eastern slopes of the northern and northern Central Andes. In contrast, up to 10 % of total DJF rainfall is accounted for by each burst in the subtropical plains (Fig. 6a).
2. LLE bursts contribute more to total DJF rainfall, with corresponding fractions between 4 and 8 % in the tropics and up to 20 % in the subtropics (Fig. 6b).
3. For SEE, we find contributions below 2 % from each burst in the Central Amazon Basin and between 6 and 10 % in northern Argentina (Fig. 6c).
4. Finally, SLE bursts contribute 2–6 % to total DJF rainfall in the tropics, and up to 20 % in the subtropics (Fig. 6d).

We note that, by dividing these values by the typical numbers of events per burst, the fraction accounted for by each single *event* can be obtained. For an integration of these fractions with respect to the mountainous catchments C1 to C7 we refer to Fig. 7.

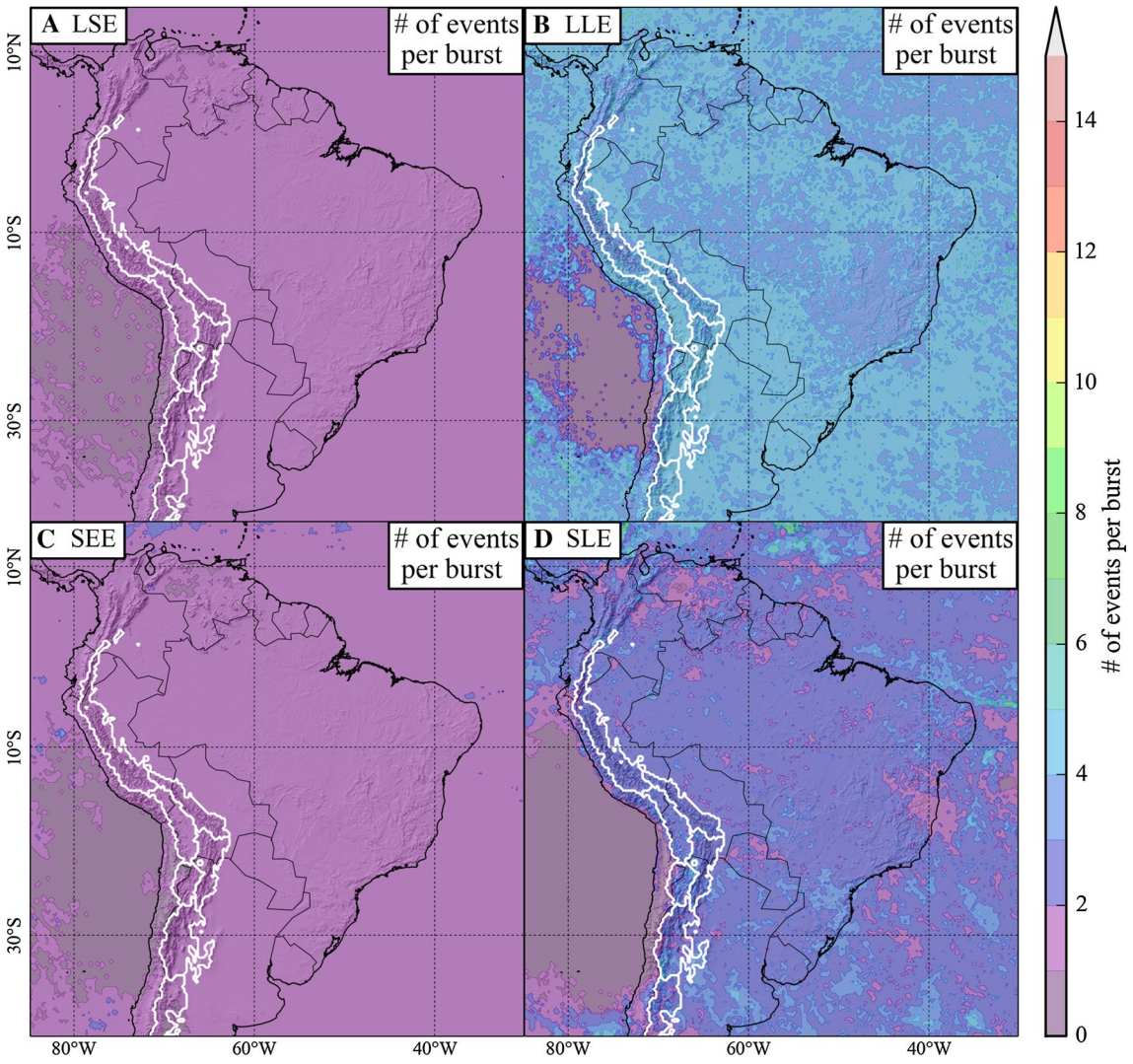

Fig. 5 Average number of 3-hourly events per burst of consecutive events of type local and short (**a** LSE), local and long-lasting (**b** LLE), spatially extensive (**c** SEE), and spatially extensive long-lasting (**d** SLE)

4.1.4 Spatial extensions

By construction, the two event types SEE and SLE involve a minimum spatial size of connected components of simultaneous events (their minimum "rainfall cluster size", S_i^q). We show this size in units of km^2, which we obtain by computing $(0.25° \times 111\text{km})^2 \times S_i^q \times \cos(\lambda)$, where $\lambda \in [-40°, 15°]$ denotes the latitudinal angle. We emphasize that the conversion from the number of grid cells to km^2 is only approximately true, since the spatial distribution of the component size thresholds is biased by the dependence of the grid cell size on the latitudinal position. We correct for this effect by weighting each threshold value with $\cos(\lambda)$.

The component size threshold for SEE (Fig. 8a) shows highest values north of the ITCZ over the tropical Atlantic Ocean and east of the Brazilian coast south of 10°S. Over southeastern South America values are smaller than in the latter regions, but still higher than over the remaining part of the continent. In contrast, SLE events (Fig. 8b) exhibit highest component size thresholds over southeastern South America, centered over Uruguay.

4.2 Regional connectivity of Andean catchments

In the second step of this study, we investigate the origins of extreme rainfall on the Altiplano-Puna Plateau (C1 and C2, Fig. 9) in Bolivia and northern Argentina as well as at the eastern foothills of the entire Andean cordillera, which we resolved with respect to the various drainage basins located along the mountain range (C3–C7, Fig. 10). We note that the network measure regional connectivity

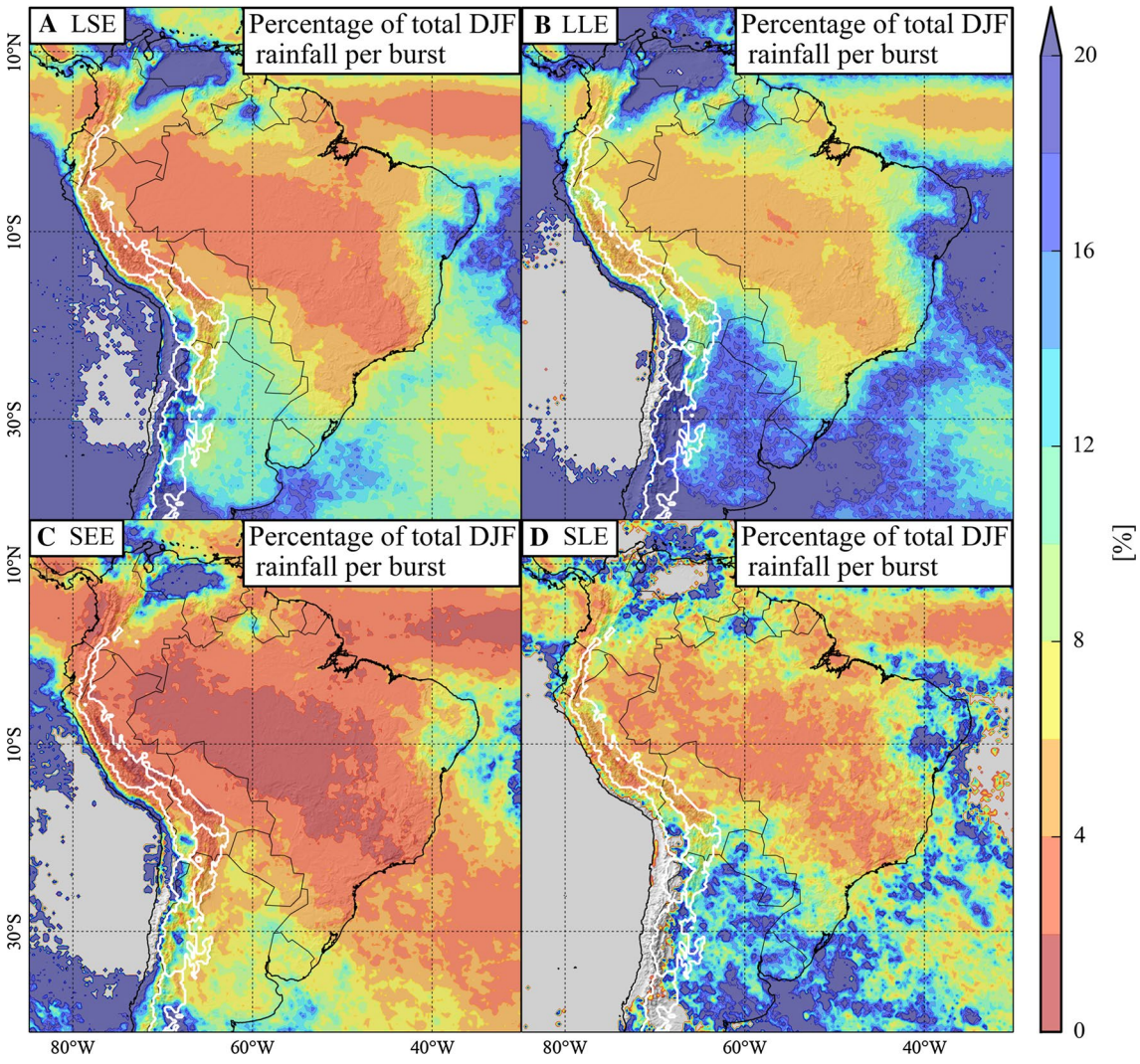

Fig. 6 Average percentage of total DJF rainfall contributed by each single burst of consecutive events of type local and short (**a** LSE), local and long-lasting (**b** LLE), spatially extensive (**c** SEE), and spatially extensive long-lasting (**d** SLE)

should not be understood in terms of single, propagating storms. Many different hydrometeoric processes control the synchronization of rainfall events, and in particular over longer spatial distances, synoptic phenomena like atmospheric waves should be taken into account as responsible mechanisms.

4.2.1 Altiplano-Puna plateau (C1 and C2)

1. For LSE, we observe almost no linkages from other regions of South America for both C1 and C2 (Fig. 9a).
2. For LLE, we observe few linkages from some scattered locations in northern Argentinean plains to C1. In contrast, we observe a large connected area over Uruguay and northern Argentina, which exhibits strong linkages into C2. Moreover, we observe linkages from C1 to C2 and vice versa (Fig. 9b).
3. For SEE, there is only a small connected area in northeastern Argentina which is linked to C1, while a large connected area extending from Uruguay to the slopes of the northern Argentinean Andes exhibits linkages into C2 (Fig. 9c).
4. For SLE, we observe two large regions which have linkages into C1: The mouth of the Amazon in northern Brazil, as well as a region east of the southern Brazilian coast. In addition to the linkages from southeastern South America to C2 which have already been found for LLE and SEE, for SLE there is also a region in northern Peru and southern Columbia which is strongly linked to C2 (Fig. 9d).

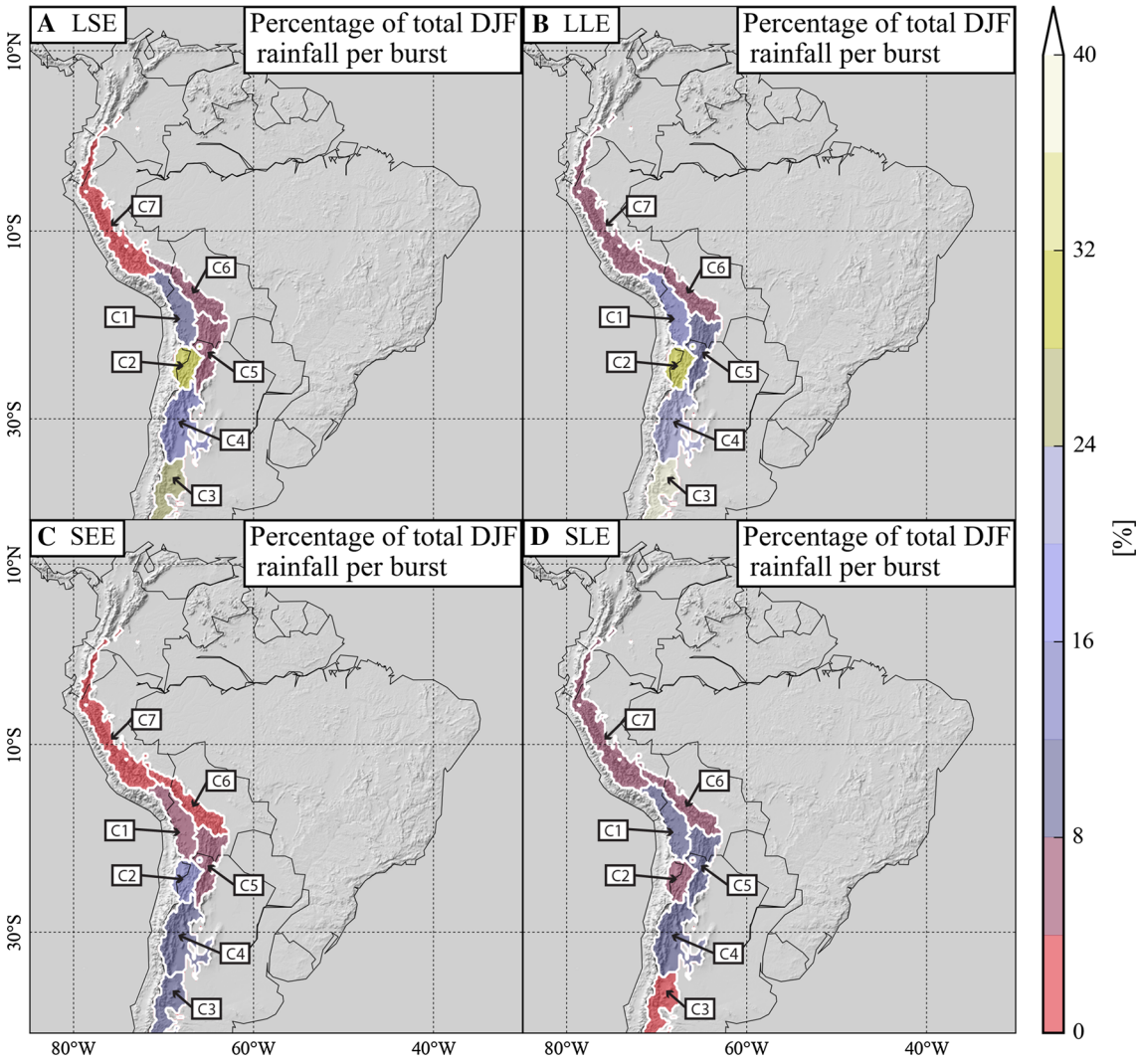

Fig. 7 Average percentage of total DJF rainfall contributed to the catchments C1 to C7 by each single burst of consecutive events of type local and short (**a** LSE), local and long-lasting (**b** LLE), spatially extensive (**c** SEE), and spatially extensive long-lasting (**d** SLE)

4.2.2 Andean foothills (C2–C7)

1. For LSE (Fig. 10a), we do not find any significant linkages into C3 and C4. C5 shows strong linkages from a large connected area in northern Argentina, Uruguay and southern Brazil, while for C6, this area is shifted northward to include Paraguay, southern Bolivia and some parts of the Bolivian part of the Amazon Basin. For C7, we observe strong linkages from the western Amazon Basin in Peru and western Brazil.
2. For LLE (Fig. 10b), there are strong linkages from central Chile and the southern Pacific ocean south of 30°S into C3, while a large connected area in central Argentina shows strong linkages into C4. C5 has strong linkages from northern Argentina and Uruguay, while for C6 and C7, we do not find significant linkages for LLE.
3. For SEE (Fig. 10c), C3 again exhibits linkages from central Chile and the adjacent Pacific Ocean, while C4 shows no significant linkages. In contrast, there are strong linkages from a large area in northern Argentina and Uruguay to C5. Furthermore, C6 shows strong linkages from a large area in Central South America, roughly extending between 10°S and 30°S and 75°W and 65°W. Strong linkages can be observed from the western Amazon Basin to C7.
4. For SLE (Fig. 10d), there are no significant linkages into C3 and C4. A large area comprised of southern Brazil, Uruguay, and northern Argentina is linked to C5, while a considerably smaller region in northern Argentina, western Paraguay, and Bolivia exhibits linkages into C6. We do not observe a large connected area with significant linkages into C7.

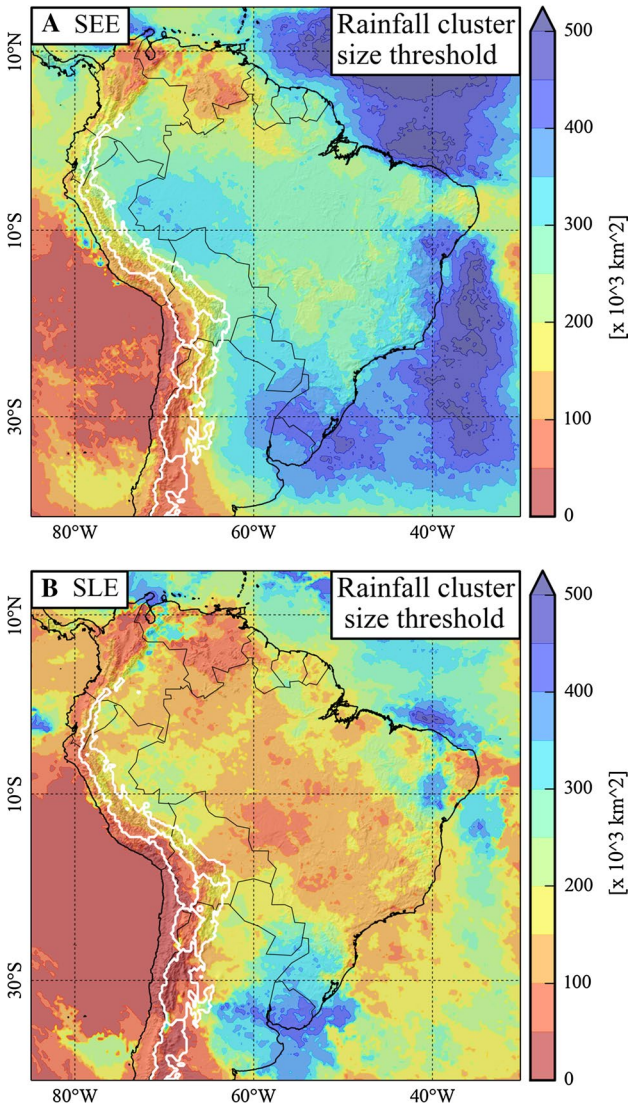

Fig. 8 **a** 90th percentiles of the sizes of connected components of simultaneous events ("cluster sizes") above the 50th percentile of local rainfall distributions confined to wet times (SEE). The size is measured in km^2 and we corrected for the bias induced by the dependence of grid cell size on latitude. B. 90th percentile of the size of connected components of simultaneous events above the 90th percentile of local 15-h smoothed rainfall distribution confined to wet times (SLE)

5 Discussion

5.1 Intensity, frequency, and spatial extent of rainfall events

By construction, the four rainfall event types LSE, LLE, SEE, and SLE occur with varying intensities (Fig. 2), frequencies (Fig. 3), and spatial extents (Fig. 8a, b). Therefore, they also play very different roles for the hydrological budgets of the different mountainous Andean catchments C1–C7. Our results indicate that LSE contributes the largest fraction of total DJF rainfall in the entire considered spatial domain, with percentages of up to 50 % in the La Plata Basin. However, in view of the induced risk of natural hazards, it is crucial to consider the temporal duration of rainfall. For this purpose, we quantified the fraction of total DJF rainfall contributed by each single sequence of consecutive events ("bursts"). For all four event types (Fig. 6), this revealed a pronounced latitudinal gradient, with lower contributions in the tropics, and higher contributions in the subtropics. Thus, there is a tendency towards low-frequency but high-magnitude events in subtropical South America. LLE and SLE contribute the largest fractions of total DJF rainfall per burst, with values close to 20 % in the northern Argentina, Uruguay, and Paraguay (Fig. 6b, d).

Mesoscale convective systems have been found to play a major role for total DJF rainfall in southeastern South America (Salio et al. 2007; Durkee and Mote 2009b), but are also important and have potentially disastrous impacts in other parts of the continent (Zipser et al. 2006). Nevertheless, they occur most frequently and attain their largest size in the subtropical regions of northern Argentina and Paraguay (Durkee et al. 2009), which is consistent with our results for the 90th percentile scores of rainfall cluster sizes (Fig. 8a, b). The hydrological role of the spatial extents of rainfall clusters can—by definition—not be directly quantified in terms of local (i.e., per grid cell) contributions to total DJF rainfall, as is also evident from the comparably low values in Fig. 6c. Nevertheless, the spatial extent is very important for the risk assessment of associated flooding and landsliding (Marengo et al. 1998; Grimm and Tedeschi 2009).

5.2 Regional connectivity of Andean catchments

In view of natural hazards such as flooding and landsliding, we expect the most severe impacts of heavy rainfall on the high-elevation Altiplano-Puna Plateau as well as in the main river catchments along the eastern foothills of the Andean cordillera.

Altiplano-Puna Plateau On the Altiplano (C1), up to 10 % of total DJF rainfall is contributed by each burst of events of type SLE, which occur less than once per DJF season. Substantial connectivity of rainfall on the Altiplano to other geographical regions is only observed for this event type. This indicates that—typically—only these largest, longest-lasting and most intense rainfall clusters synchronize with events of similar characteristics on the northern part of the plateau on more than 4 km elevation, while the remaining three types of events do not occur in a spatially connected manner, but are controlled rather locally. The most pronounced geographical source region for SLE on the Altiplano is located in northern Brazil and extends with lower connectivity westward to the Amazon Basin.

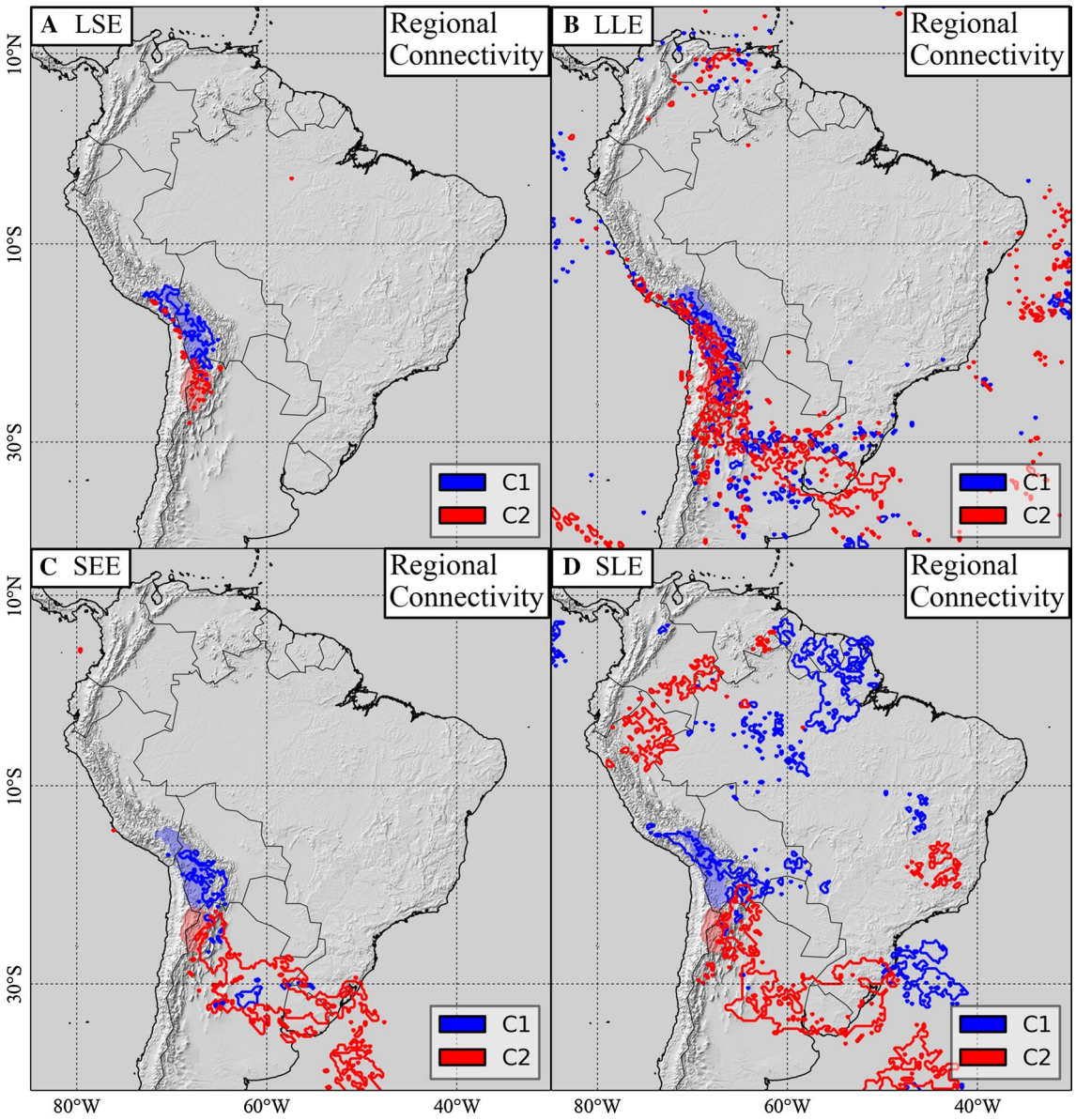

Fig. 9 Regional Connectivity of the Altiplano (C1 in *blue*) and Puna Plateau (C2 in *red*) for local and short extreme events (**a** LSE), local and long-lasting extreme events (**b** LLE), spatially extensive events (**c** SEE), and spatially extensive long-lasting extreme events (**d** SLE). Spatially extensive, long-lasting extreme events (SLE) on the northern Altiplano Plateau (*blue*) are primarily connected to the Amazon Basin, while the southern Puna Plateau (*red*) is more strongly connected to the Argentinean plains and La Plata river basin

We associate this pattern with large Amazonian squall lines, which are related to an intensification of the low-level easterlies due to easterly waves and a localized heat source over the western Amazon (Cohen et al. 1995). These features thus appear to lead to conditions favorable for the formation of SLE on the Altiplano (Fig. 9). The latter pattern is thus an example where regional connectivity cannot be interpreted in terms of propagating storm systems, but rather in terms of indirect atmospheric forcings.

As for the Altiplano, LSE in the Puna de Atacama typically occur locally, without strongly synchronized events at other locations. In strong contrast, rainfall of type LLE, SEE, and SLE in the Puna de Atacama (C2) is mainly influenced by systems originating from southeastern South America. We associate this propagation of extreme, long lasting and spatially extensive rainfall from southeastern South America to the southern part of the Altiplano-Puna Plateau with frontal systems approaching from the south (Boers et al. 2014a), caused by midlatitude cyclones and Rossby-wave activity (Hoskins and Ambrizzi 1993). This propagation pattern is also related to a subclass of mesoscale convective systems, which propagate from the

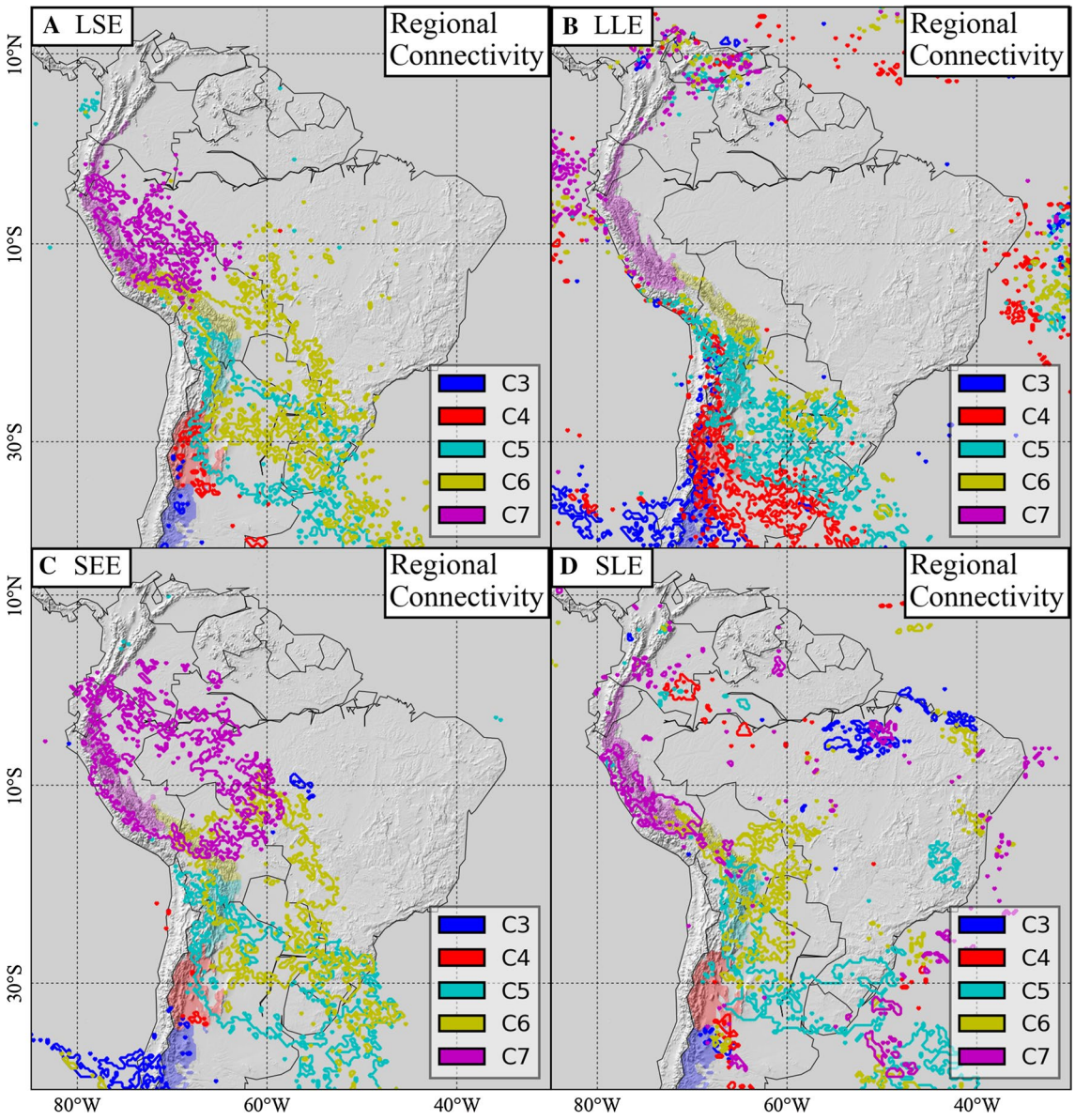

Fig. 10 Regional Connectivity of the five mountainous catchments along the eastern Andean slopes (C3–C7) for local and short extreme events (**a** LSE), local and long-lasting extreme events (**b** LLE), spatially extensive events (**c** SEE), and spatially extensive long-lasting extreme events (**d** SLE). In general, extreme rainfall in the northern Andean catchments (*purple*) are mostly locally connected, only SEE are influenced by the western Amazon basin. Tropical northern central Andean catchments (*yellow*) are impacted by rainfall events originating from southeastern South America and the southwestern Amazon Basin; Subtropical southern central Andean catchments (*green*) are dominated by rainfall originating from southeastern South America and propagating westward through the La Plata basin. Subtropical catchments to the south of the central Andes (*red* and *blue*) show only connections to extratropical regions

subtropical plains towards the southern Central Andes, i.e. in opposite direction of the northeasterly low-level moisture flow from the tropics (Anabor et al. 2008). Favorable atmospheric conditions for these propagation patterns are probably related to so-called *cold surges* (Garreaud and Wallace 1998; Garreaud 2000; Boers et al. 2014a). It is remarkable that the frontal systems exhibit such a strong impact on large areas at elevations above 4 km asl. We also note that SLE on the Puna de Atacama are—in addition to the source region in southeastern South America—connected to preceding events in northern Peru and Colombia (Fig. 9). We are not aware of a specific known climatological mechanism behind the latter feature, and intend to investigate this in future work.

Andean foothills Events of type LSE and SLE at the eastern foothills of the Andes south of 25°S (C3 and C4) do not show significant linkages to other geographical regions. In contrast, LLE and SEE at the eastern slopes of

the southern Andes (C3) are associated with events over the adjacent Pacific Ocean. Extreme rainfall at the western slopes of the southern Andes can be explained by the interplay of frontal systems migrating eastward over the southern Pacific and the Andean orogen (Garreaud 2009). Our results suggest that the frontal influence extends eastward beyond the Andean mountain range and causes long-lasting (LLE) and spatially extensive (SEE) rainfall events in these regions (Fig. 10). This is consistent with studies on the influence of baroclinic systems on convection in subtropical South America (Salio et al. 2007; Romatschke and Houze 2010; Rasmussen and Houze 2011).

LLE at the southern Central Andean foothills (C4) originate from the Argentinean lowlands and the adjacent Atlantic Ocean to the east. As in the case of the Puna de Atacama, we explain this pattern with frontal systems approaching from the south and migrating northward over South America east of the Andes. The Central Andean slopes (C5) in northern Argentina and southern Bolivia are strongly impacted by these frontal systems and associated cold surges, which also influence the formation and propagation of mesoscale convective systems (Anabor et al. 2008; Boers et al. 2014a).

For all four event types, we observe large connected geographical source regions over northern Argentina, Uruguay, and southern Brazil. This is consistent with an earlier study on the propagation of large rainfall clusters from southeastern South America towards the Central Andes (Boers et al. 2014a).

For the northern Central Andean foothills (C6), the influence of frontal systems is substantially reduced for LLE and SLE, while for LSE and SEE, we still observe large connected source regions in Bolivia, Paraguay, and northern Argentina. However, these source regions are shifted northward when compared to the source regions of the Central Andes and also extend towards the Bolivian and Brazilian Amazon Basin. We suggest that this pattern may in fact be comprised of different meteorological signals, including northward migrating frontal systems and southwestward propagating rainfall clusters originating from the tropics. The fact that there are no strong linkages for LLE and SLE suggests that those events at the northern Central Andean foothills which are caused by these subtropical frontal systems and tropical rainfall clusters on average only attain temporal durations below 12 h (the typical time scale of LLE).

In strong contrast to the catchments in the southern and central Andes, the northern Andean foothills (C7, north of 15°) do not show any linkage with frontal systems propagating over subtropical South America. Instead, we find that LSE and SEE in this area originate from the western Amazon Basin, while LLE and SLE are not linked to other geographical locations. This suggests that long-ranged linkages of rainfall at the northern Andean slopes only occur for short-lived events. In contrast, long-lasting rainfall events in this region occur at more local spatial scales.

6 Conclusion

We have analyzed the frequency, duration, spatial extent, and spatial synchronization structure of 3-h rainfall events during the South American monsoon season. For this purpose, we have defined four different types of rainfall: (1) events which are characterized by their high intensity alone; (2) long-lasting and intense events; (3) spatially extensive events; and (4) intense, long-lasting and spatially extensive events. We have focussed on the contributions of these events to total seasonal rainfall sums, and—in view of possible predictability—their geographical origins over the South American continent. These source regions are determined by a recently introduced methodology based on complex network theory and a non-linear measure of synchronization of events at different locations.

Our key findings can be summarized as follows: (1) The overall contribution to total monsoon-seasonal rainfall is highest for events of type (1). However, taking into account the temporal duration of events reveals that large river catchments in the subtropical Argentinean plains are exposed to rare, long-lasting episodes of intense and spatially extensive rainfall, each of them contributing up to 20 % to total seasonal rainfall. (2) The high-elevation Altiplano Plateau in Bolivia and southern Peru is only reached by the largest, longest-lasting and most intense thunderstorms originating from the eastern Amazon Basin. (3) For extreme events in the various river catchments along the mountainous Andes, we observe a clear transition regarding their geographical origin: While in the catchments south of 20°S, including the Puna Plateau, extreme rainfall originates from frontal systems approaching from the central Argentinean plains, the catchments north of 20°S, including the Altiplano Plateau, are mainly affected by squall lines originating from the Amazon Basin.

Acknowledgments This paper was developed within the scope of the IRTG 1740/TRP 2011/50151-0, funded by the DFG/FAPESP. JK acknowledges financial support from the Government of the Russian Federation (Agreement No. 14.Z50.31.0033). Computations were performed with the IBM iDataPlex Cluster at the Potsdam Institute for Climate Impact Research. The TRMM 3B42 V7 data are available at http://disc.sci.gsfc.nasa.gov/gesNews/trmm_v7_multisat_precip.

References

Anabor V, Stensrud DJ, de Moraes OLL (2008) Serial upstream-propagating mesoscale convective system events over southeastern

South America. Mon Weather Rev 136(8):3087–3105. doi:10.1175/2007MWR2334.1
Barros VR, Clarke R, Silva Días P (2006) Climate Change in the La Plata Basin. Consejo Nacional de Investigaciones Científicas y Técnicas
Berezin Y, Gozolchiani A, Guez O, Havlin S (2012) Stability of climate networks with time. Sci Rep 2:1–8
Boers N, Bookhagen B, Marwan N, Kurths J, Marengo J (2013) Complex networks identify spatial patterns of extreme rainfall events of the South American Monsoon System. Geophys Res Lett 40(16):4386–4392. doi:10.1002/grl.50681
Boers N, Bookhagen B, Barbosa HMJ, Marwan N, Kurths J, Marengo J (2014a) Prediction of extreme floods in the eastern central andes based on a complex network approach. Nat Commun 5:5199. doi:10.1038/ncomms6199
Boers N, Donner RV, Bookhagen B, Kurths J (2014b) Complex network analysis helps to identify impacts of the El Niño Southern Oscillation on moisture divergence in South America. Clim Dyn. doi:10.1007/s00382-014-2265-7
Boers N, Rheinwalt A, Bookhagen B, Barbosa HMJ, Marwan N, Marengo JA, Kurths J (2014c) The South American rainfall dipole: a complex network analysis of extreme events. Geophys Res Lett 41(20):1944–8007. doi:10.1002/2014GL061829
Boers N, Bookhagen B, Marengo J, Marwan N, v Sorch JS, Kurths J (2015) Extreme rainfall of the South American monsoon system: a dataset comparison using complex networks. J Clim 28(3):1031–1056. doi:10.1175/JCLI-D-14-00340.1
Bookhagen B, Strecker MR (2008) Orographic barriers, high-resolution TRMM rainfall, and relief variations along the eastern Andes. Geophys Res Lett 35(6):L06,403
Bookhagen B, Strecker MR (2012) Spatiotemporal trends in erosion rates across a pronounced rainfall gradient: examples from the southern Central Andes. Earth Planet Sci Lett 327–328:97–110. doi:10.1016/j.epsl.2012.02.005
Carvalho LMV, Jones C, Posadas AND, Quiroz R, Bookhagen B, Liebmann B (2012) Precipitation characteristics of the South American monsoon system derived from multiple datasets. J Clim 25(13):4600–4620. doi:10.1175/JCLI-D-11-00335.1
Chen S, Hong Y, Gourley JJ, Huffman GJ, Tian Y, Cao Q, Yong B, Kirstetter PE, Hu J, Hardy J, Li Z, Khan SI, Xue X (2013) Evaluation of the successive V6 and V7 TRMM multisatellite precipitation analysis over the Continental United States. Water Resourc Res 49(12):8174–8186. doi:10.1002/2012WR012795
Cohen JCP, Silva Dias MAFS, Nobre CA (1995) Environmental conditions associated with Amazonian Squall Lines: a case study. Mon Weather Rev 123(11):3163–3174
Donges JF, Zou Y, Marwan N, Kurths J (2009) The backbone of the climate network. Europhys Lett 87(4):48,007
Durkee JD, Mote TL (2009a) A climatology of warm-season mesoscale convective complexes in subtropical South America. Int J Climatol. doi:10.1002/joc.1893
Durkee JD, Mote TL (2009b) A climatology of warm-season mesoscale convective complexes in subtropical South America. Int J Climatol 30(3):418–431
Durkee JD, Mote TL (2009c) A climatology of warm?season mesoscale convective complexes in subtropical South America. Int J Climatol 30(3):418–431. doi:10.1002/joc
Durkee JD, Mote TL, Shepherd JM (2009) The contribution of mesoscale convective complexes to rainfall across subtropical South America. J Clim 22(17):4590–4605. doi:10.1175/2009JCLI2858.1
Farr TG, Rosen PA, Caro E, Crippen R, Duren R, Hensley S, Kobrick M, Paller M, Rodriguez E, Roth L, Seal D, Shaffer S, Shimada J, Umland J, Werner M, Oskin M, Burbank D, Alsdorf DE (2007) The shuttle radar topography mission. Rev Geophys 45(2). doi:10.1029/2005RG000183
Garreaud RD (2000) Cold air incursions over subtropical South America: mean structure and dynamics. Mon Weather Rev 128(7):2544–2559. doi:10.1175/1520-0493(2000)128<2544:CAIOSS>2.0.CO;2
Garreaud RD (2009) The Andes climate and weather. Adv Geosci 22:1–9. doi:10.5194/adgeo-22-3-2009
Garreaud RD, Aceituno P (2001) Interannual rainfall variability over the South American Altiplano. J Clim 14(12):2779–2789
Garreaud RD, Wallace JM (1998) Summertime incursions of midlatitude air into subtropical and tropical South America. Mon Weather Rev 126(10):2713–2733. doi:10.1175/1520-0493(1998)126<2713:SIOMAI>2.0.CO;2
Garreaud RD, Vuille M, Clement AC (2003) The climate of the Altiplano: observed current conditions and mechanisms of past changes. Palaeogeogr Palaeoclimatol Palaeoecol 194(1):5–22
Griffiths PG, Magirl CS, Webb RH, Pytlak E, Troch Pa, Lyon SW (2009) Spatial distribution and frequency of precipitation during an extreme event: July 2006 mesoscale convective complexes and floods in southeastern Arizona. Water Resourc Res 45(7):W07,419. doi:10.1029/2008WR007380
Grimm AM, Tedeschi RG (2009) ENSO and extreme rainfall events in South America. J Clim 22(7):1589–1609. doi:10.1175/2008JCLI2429.1
Harden CP (2006) Human impacts on headwater fluvial systems in the northern and central Andes. Geomorphology 79:249–263. doi:10.1016/j.geomorph.2006.06.021
Hoskins BJ, Ambrizzi T (1993) Rossby wave propagation on a realistic longitudinally varying flow. J Atmos Sci 50(12):1661–1671. doi:10.1175/1520-0469(1993)050<1661:RWPOAR>2.0.CO;2
Houze Jr RA (2012) Orographic effects on precipitating clouds. Rev Geophys 1–47. doi:10.1029/2011RG000365.1.INTRODUCTION
Huffman G, Bolvin D, Nelkin E, Wolff D, Adler R, Gu G, Hong Y, Bowman K, Stocker E (2007) The TRMM multisatellite precipitation analysis (TMPA): Quasi-global, multiyear, combined-sensor precipitation estimates at fine scales. J Hydrometeorol 8(1):38–55. doi:10.1175/JHM560.1
Khan S, Kuhn G, Ganguly AR, Erickson DJ, Ostrouchov G (2007) Spatio-temporal variability of daily and weekly precipitation extremes in South America. Water Resourc Res 43(11):1–25. doi:10.1029/2006WR005384
Maddox RA (1980) Mesoscale convective complexes. Bull Am Meteorol Soc 61(11):1374–1387
Malik N, Bookhagen B, Marwan N, Kurths J (2012) Analysis of spatial and temporal extreme monsoonal rainfall over South Asia using complex networks. Clim Dyn 39(3):971–987. doi:10.1007/s00382-011-1156-4
Marengo JA, Tomasella J, Uvo CR (1998) Trends in streamflow and rainfall in tropical South America: amazonia, eastern Brazil, and northwestern Peru. J Geophys Res 103(D2):1775–1783. doi:10.1029/97JD02551
Marengo JA, Soares WR, Saulo C, Nicolini M (2004) Climatology of the low-level jet east of the Andes as derived from the NCEP-NCAR reanalyses: characteristics and temporal variability. J Clim 17(12):2261–2280. doi:10.1175/1520-0442(2004)017<2261:COTLJE>2.0.CO;2
Messerli B, Grosjean M, Vuille M (1997) Water availability, protected areas, and natural resources in the Andean desert altiplano. Mt Res Dev 17(3):229–238
Moreiras SM (2005) Climatic effect of ENSO associated with landslide occurrence in the Central Andes, Mendoza Province, Argentina. Landslides 2:53–59. doi:10.1007/s10346-005-0046-4
Papalexiou SM, Koutsoyiannis D (2013) Battle of extreme value distributions: a global survey on extreme daily rainfall. Water Resourc Res 49(1):187–201. doi:10.1029/2012WR012557

Poveda G, Jaramillo L, Vallejo LF (2014) Seasonal precipitation patterns along pathways of South American low-level jets and aerial rivers. Water Resourc Res 50(1):98–118. doi:10.1002/2013WR014087

Programa de las Naciones Unidas para el Desarrollo (PNUD) (2011) Tras las huellas del cambio climático en Bolivia

Quiroga RQ, Kreuz T, Grassberger P (2002) Event synchronization: a simple and fast method to measure synchronicity and time delay patterns. Phys Rev E 66(4):041,904

Radebach A, Donner RV, Runge J, Donges JF, Kurths J (2013) Disentangling different types of El Niño episodes by evolving climate network analysis. Phys Rev E 88(052):807. doi:10.1103/PhysRevE.88.052807

Rasmussen KL, Houze RA (2011) Orogenic convection in subtropical South America as seen by the TRMM satellite. doi:10.1175/MWR-D-10-05006.1

Renard B, Kochanek K, Lang M, Garavaglia F, Paquet E, Neppel L, Najib K, Carreau J, Arnaud P, Aubert Y, Borchi F, Soubeyroux JM, Jourdain S, Veysseire JM, Sauquet E, Cipriani T, Auffray A (2013) Data-based comparison of frequency analysis methods: a general framework. Water Resourc Res 49(2):825–843. doi:10.1002/wrcr.20087

Rheinwalt A, Boers N, Marwan N, Kurths J, Gerstengarbe FW, Werner P (2014) Non-linear time series analysis of precipitation events using regional climate networks for the region of Germany. Clim Dyn (under review)

Romatschke U, Houze RA (2010) Extreme summer convection in South America. J Clim 23:3761–3791. doi:10.1175/2010JCLI3465.1

Romatschke U, Houze RA (2013) Characteristics of precipitating convective systems accounting for the summer rainfall of tropical and subtropical South America. J Hydrometeorol 14(1):25–46. doi:10.1175/JHM-D-12-060.1

Salio P, Nicolini M, Zipser EJ (2007) Mesoscale convective systems over southeastern South America and their relationship with the South American low-level jet. Mon Weather Rev 135(4):1290–1309. doi:10.1175/MWR3305.1

Serinaldi F, Kilsby CG (2014) Rainfall extremes: toward reconciliation after the battle of distributions. Water Resourc Res 50(1):336–352. doi:10.1002/2013WR014211

Steinhaeuser K, Ganguly AR, Chawla NV (2012) Multivariate and multiscale dependence in the global climate system revealed through complex networks. Clim Dyn 39(3–4):889–895. doi:10.1007/s00382-011-1135-9

Stolbova V, Martin P, Bookhagen B, Marwan N, Kurths J (2014) Topology and seasonal evolution of the network of extreme precipitation over the Indian subcontinent and Sri Lanka. Nonlinear Process Geophys 21:901–917

Tsonis AA, Swanson KL, Roebber PJ (2006) What do networks have to do with climate? Bull Am Meteorol Soc 87(5):585–595. doi:10.1175/BAMS-87-5-585

Velasco I, Fritsch JM (1987) Mesoscale convective complexes in the Americas. doi:10.1029/JD092iD08p09591

Vera C, Higgins W, Amador J, Ambrizzi T, Garreaud RD, Gochis D, Gutzler D, Lettenmaier D, Marengo JA, Mechoso CR, Nogues-Paegle J, Silva Dias P, Zhang C (2006) Toward a unified view of the American monsoon systems. J Clim 19(20):4977–5000. doi:10.1175/JCLI3896.1

Vuille M (1999) Atmospheric circulation over the Bolivian Altiplano during dry and wet periods and extreme phases of the Southern Oscillation. Int J Climatol 19(14):1579–1600

Xue X, Hong Y, Limaye AS, Gourley JJ, Huffman GJ, Khan SI, Dorji C, Chen S (2013) Statistical and hydrological evaluation of TRMM-based multi-satellite precipitation analysis over the Wangchu Basin of Bhutan: are the latest satellite precipitation products 3B42V7 ready for use in ungauged basins? J Hydrol 499(0):91–99. doi:10.1016/j.jhydrol.2013.06.042

Yamasaki K, Gozolchiani A, Havlin S (2008) Climate networks around the globe are significantly affected by El Nino. Phys Rev Lett 100(22):228,501

Zhou J, Lau KM (1998) Does a monsoon climate exist over South America? J Clim 11(5):1020–1040

Zipser EJ, Cecil DJ, Liu C, Nesbitt SW, Yorty DP (2006) Where are the most intense thunderstorms on earth? Bull Am Meteorol Soc 87(8):1057–1071. doi:10.1175/BAMS-87-8-1057

Zulkafli Z, Buytaert W, Onof C, Manz B, Tarnavsky E, Lavado W, Guyot JL (2014) A comparative performance analysis of TRMM 3B42 (TMPA) versions 6 and 7 for hydrological applications over Andean-Amazon river basins. J Hydrometeorol 15(2):581–592. doi:10.1175/JHM-D-13-094.1